Mem. S.A.It. Vol. 82, 581

Memorie della

Simulation of the large scale structure of the Universe: shock waves and nonthermal effects

D. Ryu[1] and H. Kang[2]

[1] Department of Astronomy and Space Science, Chungnam National University, Daejeon 305-764, Korea, e-mail: ryu@canopus.cnu.ac.kr
[2] Department of Earth Sciences, Pusan National University, Pusan 609-735, Korea

Abstract. Shock waves form in the intergalactic medium (IGM) as a consequence of accretion, merger, and turbulent motions during the structure formation of the universe. The gravitational energy released during the formation is transferred to the intergalactic gas by these shocks. They not only heat gas but also govern nonthermal processes through the acceleration of cosmic rays, production of magnetic fields, and generation of vorticity. Yet, their nature remains largely unknown, because observation of shocks in the IGM is still challenging and scarce. On the other hand, simulation for the formation of the large-scale structure has revealed the general properties of cosmological shocks. Here, we briefly summarize the results from simulation, focusing mainly on cosmological shocks and diffusive shock acceleration.

Key words. Cosmic rays – Cosmology: large-scale structure of Universe – Shock waves

1. Introduction

Shock waves are ubiquitous in astrophysical environments; it was predicted that they form even in tenuous gas in the large-scale structure (LSS) of the universe (Miniati et al. 2000; Ryu et al. 2003). In the current paradigm of the cold dark matter (CDM) cosmology, the LSS of the universe forms through hierarchical clustering of matter. Deepening of gravitational potential wells causes gas to move supersonically. Cosmological shocks are induced when the gas accretes onto clusters, filaments, and sheets, or as a consequence of subclump merger and turbulent flow motions inside the nonlinear structures.

Shock waves in the LSS of the universe have been studied in details using various hydrodynamic simulations for the cold dark matter cosmology with cosmological constant (ΛCDM) (Ryu et al. 2003; Pfrommer et al. 2006; Kang et al. 2007; Skillman et al. 2008; Hoeft et al. 2008; Vazza et al. 2009). Shocks with Mach number up to $M \sim 10^4$ and speed up to $V_s \sim$ a few $\times 1000\,\mathrm{km\,s^{-1}}$ may exist in the present universe ($z = 0$). In the hot intracluster media (ICMs) and cluster outskirts, however, shocks form with $M \lesssim$ a few, and they are energetically most important and responsible for most of shock dissipation. The properties of cosmological shocks found in various simulations by different authors are generally in good agreement.

The galaxy distribution exhibits clusters and filaments, the so-called 'cosmic web',

Send offprint requests to: D. Ryu

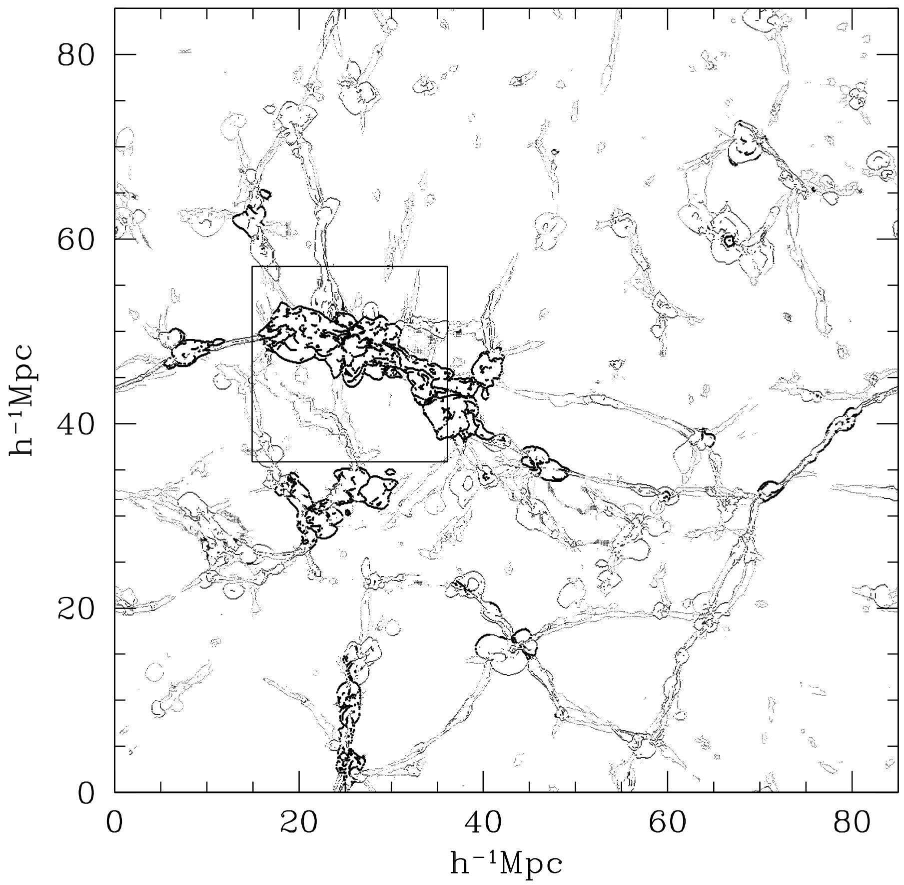

Fig. 1. Two-dimensional slice of (85 h^{-1}Mpc)^2 showing shock locations at $z = 0$. The size of points is commensurate with the shock speed. A blown-up image of the box around two merging clusters is shown in Fig. 2.

which traces the underlying distribution of matter in the LSS of the Universe (Bond et al. 1996). The cosmic web is filled with ionized plasmas, the intergalactic medium (IGM); the hot gas with $T > 10^7$ K is found in the ICMs and cluster outskirts, and the Warm Hot Intergalactic Medium (WHIM) with 10^5 K $< T < 10^7$ K is distributed mostly in filaments (Cen & Ostriker 1999; Kang et al. 2005). The diffuse gas with $T < 10^5$ K resides mainly in sheetlike structures and voids. In the following, we discuss the properties of cosmological shocks in the ICMs and cluster outskirts with $T > 10^7$ K.

2. Shocks in LSS

The results reported here are based on a simulation previously presented in Cen & Ostriker (2006) and Kang et al. (2007). The WMAP1-normalized ΛCDM cosmology was employed with the following parameters: $\Omega_b = 0.048$, $\Omega_m = 0.31$, $\Omega_\Lambda = 0.69$, $h \equiv H_0/(100$ km/s/Mpc) $= 0.69$, $\sigma_8 = 0.89$, and $n = 0.97$. The simulation was performed using a PM/Eulerian hydrodynamic cosmology code (Ryu et al. 1993). Detailed descriptions for numerical set-up and input physical ingredients can be found in Cen & Ostriker (2006). Shock waves were identified in the simulation volume

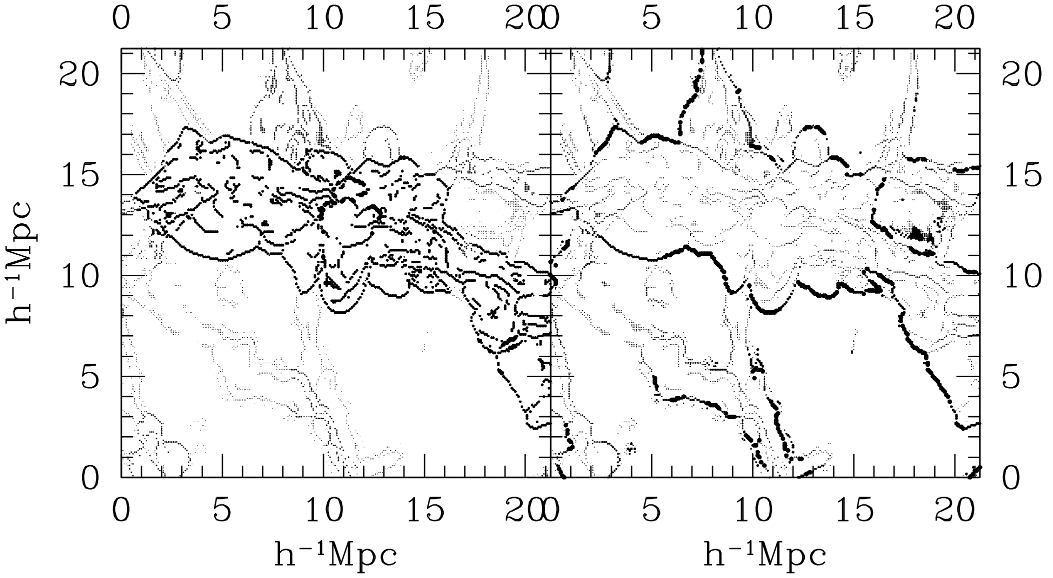

Fig. 2. Two-dimensional slice of (21.25 h^{-1}Mpc)^2 around two merging clusters of kT $\sim$ a few keV showing shock locations at z = 0. Left: The size of points is commensurate with the shock speed. Right: The size of points is commensurate with the shock Mach number.

in a post-processing analysis. The procedure to identify shocks was described in details in Ryu et al. (2003). To avoid confusion from complex flow patterns and shock surface topologies associated with very weak shocks, only those portions of shock surfaces with $M \geq 1.5$ were kept and used for the analysis of shocks properties.

Figure 1 shows the locations of identified shocks in a two-dimensional slice at $z = 0$. External accretion shocks encompass nonlinear structures and reveal, in addition to cluster complexes, rich topology of filamentary and sheet-like structures in the LSS. They form when the cold gas of $T \sim 10^4$ K in void regions accretes onto the nonlinear structures. Inside the nonlinear structures, there exist complex networks of internal shocks that form by infall of previously shocked gas to filaments and knots and during subclump mergers, as well as by chaotic flow motions. The shock-heated gas around clusters extends out to $\sim 5\ h^{-1}$Mpc, much further out than the observed X-ray emitting volume.

Figure 2 shows the shock locations around a cluster complex in the small box in Fig. 1. The region contains two clusters/groups with kT $\sim$ a few keV in the process of merging. The figure indicates that the shocks found in the ICMs and cluster outskirts have high speed (left panel) but low Mach number (right panel). It is because the shocks form in the hot gas of $kT \gtrsim$ a few keV.

The left panels of Fig. 3 show the surface area of the identified shocks in the entire simulation volume, normalized by the volume, per logarithmic Mach number interval, $dS(M)/d\log M$ (top), and per logarithmic shock speed interval, $dS(V_s)/d\log V_s$ (bottom), at $z = 0$. Here, S is given in units of $(h^{-1}\mathrm{Mpc})^{-1}$. The quantity S provides a measure of shock frequency or the inverse of the mean comoving distance between shock surfaces. Shocks with Mach number $M \lesssim$ a few and speed $V_s \sim 100\ \mathrm{km\,s^{-1}}$ are most common,

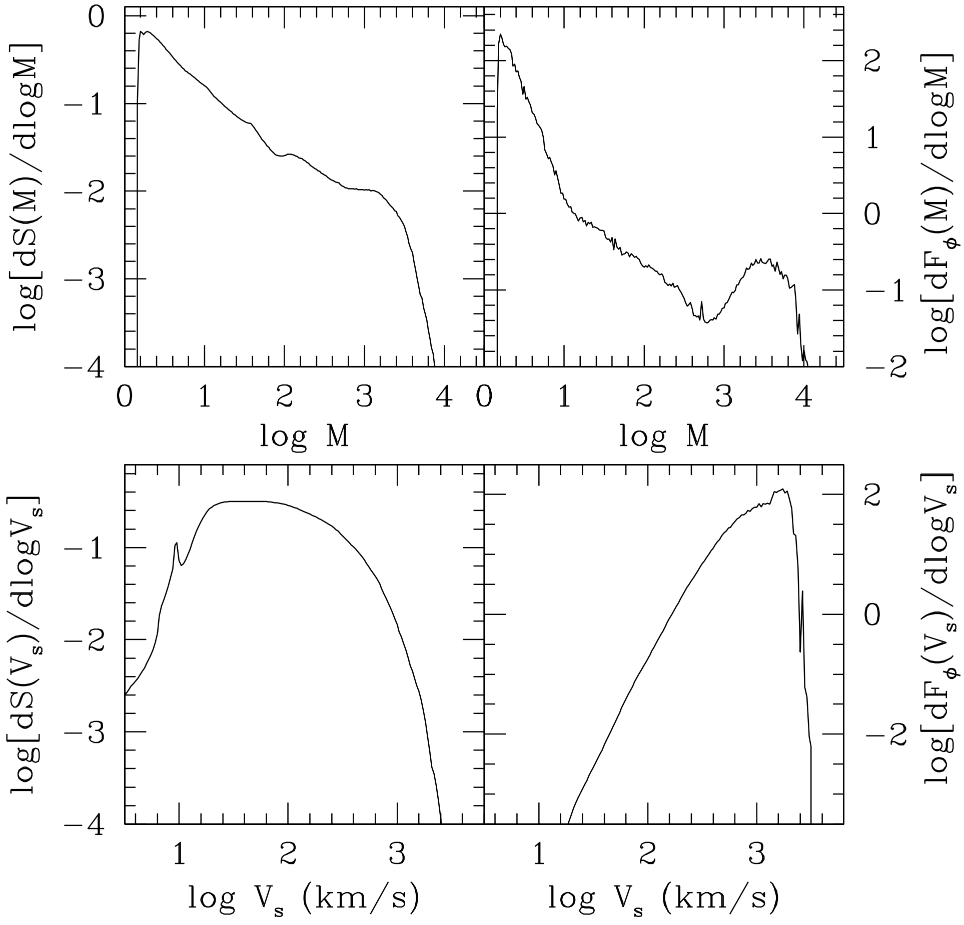

Fig. 3. Statistics of all shocks formed inside the entire simulation volume. Left: Inverse of the mean comoving distance between shock surfaces, or frequency of shocks, as a function of shock Mach number M (top) and shock speed V_s (bottom) at z = 0. Right: Kinetic energy flux per comoving volume passing through shock surfaces in units of 10^{40} ergs s^{-1} (h^{-1}Mpc)$^{-3}$ as a function of M (top) and V_s (bottom).

but shocks with up to $M \sim 10^4$ and up to $V_s \sim$ a few $\times 1000$ km s^{-1} are also present.

For identified shocks, we calculated the incident shock kinetic energy flux, $F_\phi = (1/2)\rho_1 V_s^3$, where ρ_1 is the preshock gas density. We then calculated the kinetic energy flux through shock surfaces, normalized by the simulation volume, per logarithmic Mach number interval, $dF_\phi(M)/d\log M$, and per logarithmic shock speed interval, $dF_\phi(V_s)/d\log V_s$. The right panels of Fig. 3 show this flux at z = 0. Energetically the most significant shocks are weak shocks with $M \lesssim 3$, but they have typically $V_s \gtrsim 1000$ km s^{-1}.

To get statistics for shocks in the ICMs and cluster outskirts, we selected the shocks with the preshock gas temperature of $T_1 > 10^7$ K, and calculated S and F_ϕ only for those shocks. Figure 4 shows the resulting S and F_ϕ as a function of M (per linear interval). As noted with Fig. 2, the Mach number of shocks formed in the ICMs and cluster outskirts is expected to be small, less than $\sim$ 3. The frequency increases to weakest possible shocks

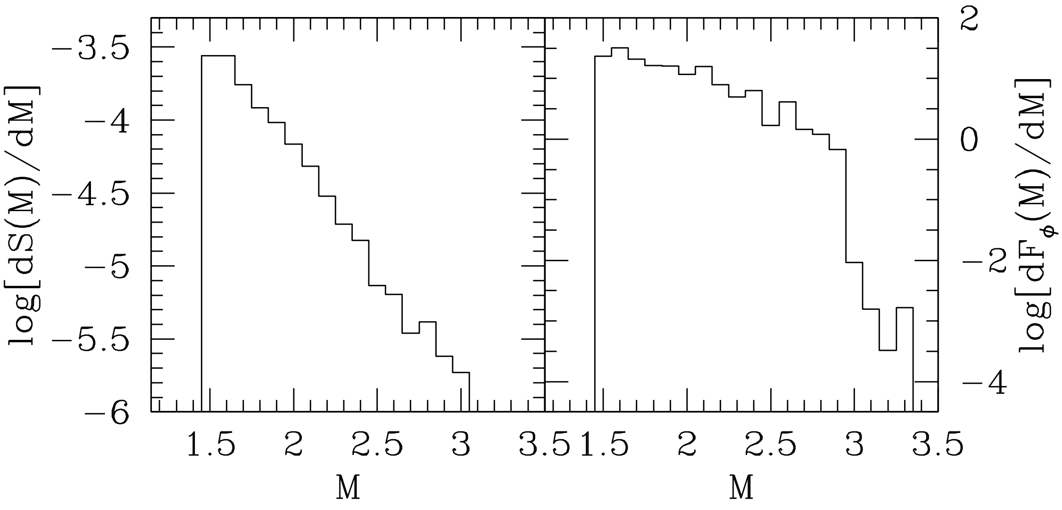

Fig. 4. Statistics of shocks in the ICMs and cluster outskirts. Left: Inverse of the mean comoving distance between shock surfaces, or frequency of shocks, as a function of shock Mach number M. Right: Kinetic energy flux per comoving volume passing through shock surfaces in units of 10^{40} ergs s^{-1} $(h^{-1}\mathrm{Mpc})^{-3}$ as a function of M.

with $M \sim 1$. The kinetic energy flux through shock surfaces is larger for weaker shocks; weaker shocks process more shock energy in the ICMs and cluster outskirts.

3. CRs accelerated at shocks

Like shock waves in other astrophysical environments, cosmological shocks are collisionless shocks that form in tenuous cosmic plasmas via collective electromagnetic interactions between gas particles and magnetic fields. They play key roles in governing the nature of ionized plasmas in the cosmic web. In addition to converting a part of the kinetic energy of bulk flow motions into the gas thermal energy, the shocks accelerate cosmic rays (CRs) by diffusive shock acceleration (DSA) (Bell 1978; Blandford & Ostriker 1978).

In DSA theory, the amount of CRs accelerated at shocks is determined mainly by the shock Mach number, while the fraction of injected CR particles plays a secondary role. At quasi-parallel shocks, some suprathermal particles into the tail of the postshock thermal distribution can leak upstream across the subshock. The injection rate, ξ, defined as the fraction of CR particles, depends on the subshock Mach number and the injection parameter, $\epsilon_B \equiv B_0/B_\perp$, that is the ratio of the mean magnetic field strength aligned with the shock normal to the amplitude of the postshock turbulent wave field. In addition, the CR population is isotropized with respect to the local Alfvénic wave turbulence, which would in general drift upstream at the Alfvén speed with respect to the bulk plasma. This reduces the velocity difference between upstream and downstream scattering centers compared to the bulk flow, leading to less efficient DSA. Moreover, the dissipation of Alfvén turbulence heats the inflowing plasma in the precursor, which leads to weakening of the subshock strength (Kang & Jones 2007).

The left panel of Fig. 5 shows the gas thermalization and CR acceleration efficiencies, defined as $\delta(M) \equiv F_{\rm th}/F_{\rm kin}$ and $\eta(M) \equiv F_{\rm CR}/F_{\rm kin}$, respectively, where $F_{\rm th}$ and $F_{\rm CR}$ are the gas thermal and CR energy flux, respectively, generated at shocks; they are from numerical simulations of quasi-parallel shocks for shock speed $v_s = M \cdot 150\,\mathrm{km\,s^{-1}}$ $(T_1 =$

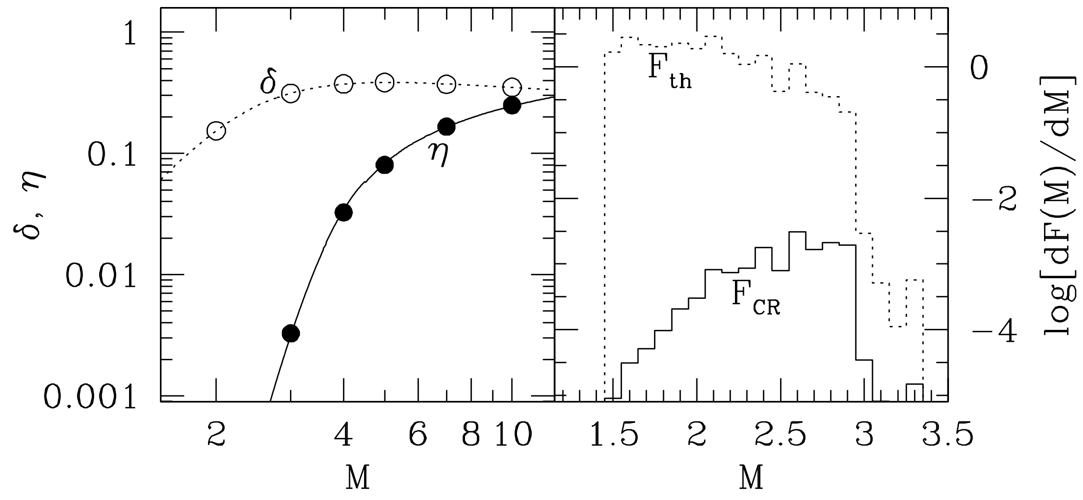

Fig. 5. Left: Gas thermalization efficiency, $\delta(M)$, and CR acceleration efficiency, $\eta(M)$, as a function of shock Mach number M. Circles are the values estimated from numerical simulations based on a DSA model and lines are the fits. Right: Gas thermal energy dissipated (dotted line) and CR energy accelerated (solid) at the shocks in the ICMs and cluster outskirts, shown in Fig. 4, a function of M. The quantities are in units of 10^{40} ergs s^{-1}(h^{-1}Mpc)$^{-3}$.

10^6K), and based on a DSA model of Kang & Jones (2007) with $\epsilon_B = 0.25$. At strong shocks with $M \gtrsim 10$, the injection rate is high enough so that the CR acceleration efficiency nearly saturates and becomes almost independent of the parameter ϵ_B. At weak shocks, on the other hand, the level of injection lies in the regime where the CR acceleration efficiency increases with the injection rate; consequently, η depends sensitively on ϵ_B. Note that the value of η presented here is $\sim 1/2$ of that presented in Kang et al. (2007) for $M \lesssim 5$, while it remains about the same for stronger shocks (see also Kang & Ryu, this conference).

By adopting the efficiencies, the gas thermal and CR energy fluxes dissipated at shocks can be calculated in the same way that the kinetic energy flux through shock surfaces is calculated. They are shown with dashed and solid lines in the right panel of Fig. 5 for shocks in the ICMs and cluster outskirts. For the generation of gas thermal energy, still weaker shocks are more important; shocks with $M \lesssim 3$ contribute most. On the other hand, the generation of CR energy is more efficient at shocks with $M \gtrsim 1.5$. This implies that in the ICMs and cluster outskirts, while shocks with $M \sim 1$ are most abundant, shocks with $1.5 \lesssim M \lesssim 3$ would be more frequently detected as radio relics.

4. Summary

Shocks are inevitable consequences of the formation of the LSS of the universe. The gravitational energy released during the structure formation is transferred by these shocks to the intergalactic gas in several different forms: heat, CRs, vorticity and turbulence, and magnetic fields. In the cosmic web, shocks with Mach number up to $M \sim 10^4$ and speed up to $V_s \sim$ a few $\times 1000$ km s^{-1} may exist in the present universe. In the ICMs and cluster outskirts, however, shocks with low Mach number of $M \lesssim 3$, but with $V_s \gtrsim 1000$ km s^{-1}, are most common; they are energetically most important and responsible for most of the dissipation of shock energy.

By applying models of DSA, we estimated CRs accelerated at shocks in the ICMs and cluster outskirts. The shocks with $M \gtrsim 1.5$ are most important in the acceleration of nonthermal particles. Our results suggest shocks with $1.5 \lesssim M \lesssim 3$ would be most frequently detected as radio relics.

Acknowledgements. DR was supported by National Research Foundation of Korea through grant 2007-0093860. HK was supported by National Research Foundation of Korea through grant 2009-0075060.

References

Bell, A. R. 1978, MNRAS, 182, 147
Bond, J. R., Kofman, L., & Pogosyan, D. 1996, Nature, 380, 603
Blandford, R. D., & Ostriker, J. P. 1978, ApJ, 221, L29
Cen, R., & Ostriker, J. P. 1999, ApJ, 514, 1
Cen, R., & Ostriker, J. P. 2006, ApJ, 650, 560
Hoeft, M., Bruggen, M., Yepes, G., Gottlober, S., & Schwope, A., 2008, MNRAS, 391, 1511
Kang, H., & Jones, T. W. 2007, Astropart. Phys., 28, 232
Kang, H., Ryu, D., Cen, R., & Ostriker, J. P. 2007, ApJ, 669, 729
Kang, H., Ryu, D., Cen, R., & Song, D. 2005, ApJ, 620, 21
Miniati, F., Ryu, D., Kang, H., Jones, T. W., Cen, R., & Ostriker, J. P. 2000, ApJ, 542, 608
Pfrommer, C., Springel, V., Enßlin, T. A., & Jubelgas, M. 2006, MNRAS, 367, 113
Ryu, D., Kang, H., Hallman, E. J., & Jones, T. W., 2003, ApJ, 593, 599
Ryu, D., Ostriker, J. P., Kang, H., & Cen, R. 1993, ApJ, 414, 1
Skillman, S. W., O'Shea, B. W., Hallman, E. J., Burns, J. O., & Norman, M. L. 2008, ApJ, 689, 1063
Vazza, F., Brunetti, G., & Gheller, C. 2009, MNRAS, 395, 1333